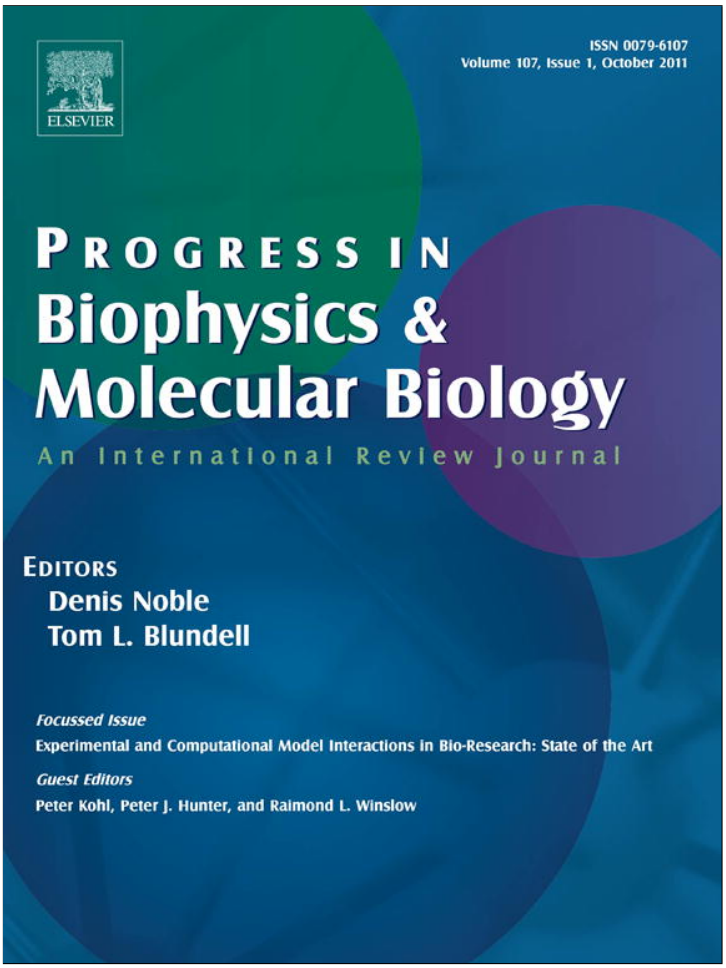

Progress in Biophysics and Molecular Biology 107 (2011) 122–133

Contents lists available at ScienceDirect

Progress in Biophysics and Molecular Biology

journal homepage: www.elsevier.com/locate/pbiomolbio

Original Research

Inter-model consistency and complementarity: Learning from *ex-vivo* imaging and electrophysiological data towards an integrated understanding of cardiac physiology

O. Camara [a,b,1,*], M. Sermesant [c,d,1], P. Lamata [d,e,1], L. Wang [f,1], M. Pop [g], J. Relan [c], M. De Craene [a,b], H. Delingette [c], H. Liu [f,h], S. Niederer [d], A. Pashaei [a,b], G. Plank [i], D. Romero [a,b], R. Sebastian [j], K.C.L. Wong [c], H. Zhang [k], N. Ayache [c], A.F. Frangi [a,b], P. Shi [f], N.P. Smith [d,e], G.A. Wright [g]

[a] *Center for Computational Imaging and Simulation Technologies in Biomedicine (CISTIB), Universitat Pompeu Fabra, Barcelona, Spain*
[b] *Networking Biomedical Research Center on Bioengineering, Biomaterials and Nanomedicine (CIBER-BBN), Barcelona, Spain*
[c] *INRIA, Asclepios Project, Sophia Antipolis, France*
[d] *Department of Biomedical Engineering, King's College London, St. Thomas Hospital, UK*
[e] *Department of Computer Science, University of Oxford, UK*
[f] *Computational Biomedicine Laboratory, Rochester Institute of Technology, Rochester, NY, USA*
[g] *University of Toronto, Sunnybrook Health Sciences Centre, Canada*
[h] *State Key Laboratory of Modern Optical Instrumentation, Zhejiang University, Hangzhou, China*
[i] *Institute of Biophysics, Medical University of Graz, Austria*
[j] *Computational Multi-Scale Physiology Lab, Universitat de Valencia, Valencia, Spain*
[k] *Chinese University of Hong Kong, Hong Kong*

ARTICLE INFO

Article history:
Available online 20 July 2011

Keywords:
Heart electrophysiology
Model integration
Optical mapping data
Parameter personalization
Phenomenological models
Fast conduction Purkinje system
Detailed ionic models
Maximum a posteriori estimation

ABSTRACT

Computational models of the heart at various scales and levels of complexity have been independently developed, parameterised and validated using a wide range of experimental data for over four decades. However, despite remarkable progress, the lack of coordinated efforts to compare and combine these computational models has limited their impact on the numerous open questions in cardiac physiology. To address this issue, a comprehensive dataset has previously been made available to the community that contains the cardiac anatomy and fibre orientations from magnetic resonance imaging as well as epicardial transmembrane potentials from optical mapping measured on a perfused *ex-vivo* porcine heart. This data was used to develop and customize four models of cardiac electrophysiology with different level of details, including a personalized fast conduction Purkinje system, a *maximum a posteriori* estimation of the 3D distribution of transmembrane potential, the personalization of a simplified reaction-diffusion model, and a detailed biophysical model with generic conduction parameters. This study proposes the integration of these four models into a single modelling and simulation pipeline, after analyzing their common features and discrepancies. The proposed integrated pipeline demonstrates an increase prediction power of depolarization isochrones in different pacing conditions.

1. Introduction

Integrative models of cardiac physiology are important for understanding disease, treatment evaluation, and intervention planning. Advances in computational physiology of the heart in recent years have improved our understanding of the pathophysiological mechanisms underlying several cardiac diseases, advancing towards a more patient-specific diagnosis with the goal of pre-operative in silico interventional planning (Smith et al., 2011).

The current state-of-the-art builds on over four decades of work developing computational models of the heart across a range of different levels of complexity and spatial-temporal scales to simulate cardiac electrical activation. The degree of complexity of the model is usually selected as a function of the targeted application and has a great impact on computational load. The interested reader is referred to a complete review of these models in Clayton

* Corresponding author. Center for Computational Imaging and Simulation Technologies in Biomedicine (CISTIB), Universitat Pompeu Fabra, Barcelona, Spain.
E-mail address: oscar.camara@upf.edu (O. Camara).
[1] The first four authors equally contributed to this manuscript, being the main author from each research centre.

0079-6107/$ – see front matter © 2011 Elsevier Ltd. All rights reserved.
doi:10.1016/j.pbiomolbio.2011.07.007

et al. (2011a). These models can be broadly categorized into two main groups: Ionic Models (IM) and Phenomenological Models (PM). IM (Noble, 1962) characterise ionic currents flowing through the cardiac cell membrane, allowing detailed modelling of events at the cellular level, using many parameters. As such, IM are not well suited for parameter personalization procedures due to computational cost limitations and the very limited availability of cellular data for an individual (Fink et al., 2011). Within PM, Eikonal Models (EM) (Keener and Sneyd, 1998) are computational efficient but simple models based on wavefront propagation and describe only the time at which a depolarization wave reaches a given point without precisely modelling the action potential. At the intermediate level are other PM such as the Mitchell–Schaeffer (MS) (Mitchell and Schaeffer, 2003), which describe the action potential generation and propagation along the cell membrane with a reduced number of ionic currents.

These model frameworks have significant potential to improve therapy planning and guidance of complex cardiology interventions such as Cardiac Resynchronization Therapy (CRT) in Heart Failure (HF) patients and Radio-Frequency Ablation (RFA) in patients suffering from Ventricular Tachycardia (VT). Both procedures have low success rates (around 30% of non-responders for CRT (Strickberger et al., 2005) and 50% for RFA of VT (Aliot et al., 2009)) due to sub-optimal patient selection and the absence of a clinical consensus on key intervention settings (e.g. optimal number and position of leads and RF ablation patterns). Thus, these interventions often involve long trial and error procedures, with the outcome being highly dependent on the experience of a specific cardiologist.

However, in order to translate simulations into a clinical context, there is an important need for personalization of such models, i.e. estimation of the model parameters which best fit patients clinical data. Using such patient-specific cardiac models, then in turn, provides a way to predict in silico the impact of different intervention settings for improved and personalized planning of these therapies.

Several authors approached personalization in cardiac models using different sources of data. For instance, patient-specific cardiac anatomy (heterogeneous tissue properties, microstructural information, coronary tree) (Sermesant et al., 2006; Camara et al., 2010c; Xi et al., 2011; Niederer et al., 2011), heart mechanics (motion/deformation/pressure) (Wang et al., 2009; Xi et al., 2011; Wong et al., 2007) provided by imaging modalities and electrophysiological information given by non-invasive electrocardiograms (Wang et al., 2010a) or invasive electrophysiological patient-specific data (Chinchapatnam et al., 2008).

However, clinical translation of these cardiac models has been hampered by the absence of complete and rigorous technical and clinical validation, as well as benchmarking of the developed tools. These are only feasible provided that benchmarking and ground-truth data capturing generic knowledge on the healthy and pathological heart is available.

To address this issue, a dataset containing the cardiac anatomy and fibre orientations from magnetic resonance images (MRI), as well as epicardial transmembrane potentials from optical mapping (Pop et al., 2009) acquired on *ex-vivo* porcine hearts, have previously been made available to the community. The obtained results, which were recently presented and discussed at the STACOM-CESC'10 workshop (Camara et al., 2010a), included: i) a new methodology to customize and regularize heart shape and myocardial fibre orientation to predict activation waves in these personalized meshes with generic conduction parameters (Lamata et al., 2010b); ii) a statistical model-constrained framework to produce *maximum a posteriori* (MAP) estimation of the 3D distribution of transmembrane potential (Wang et al., 2010b); iii) a personalized simplified reaction-diffusion 3D electrophysiological model (Mitchell-Schaeffer) (Relan et al., 2010a,b); iv) a personalized fast conduction Purkinje system (regional density of terminals and latest endocardial activation) with a simple Eikonal-based electrophysiological model (Camara et al., 2010b).

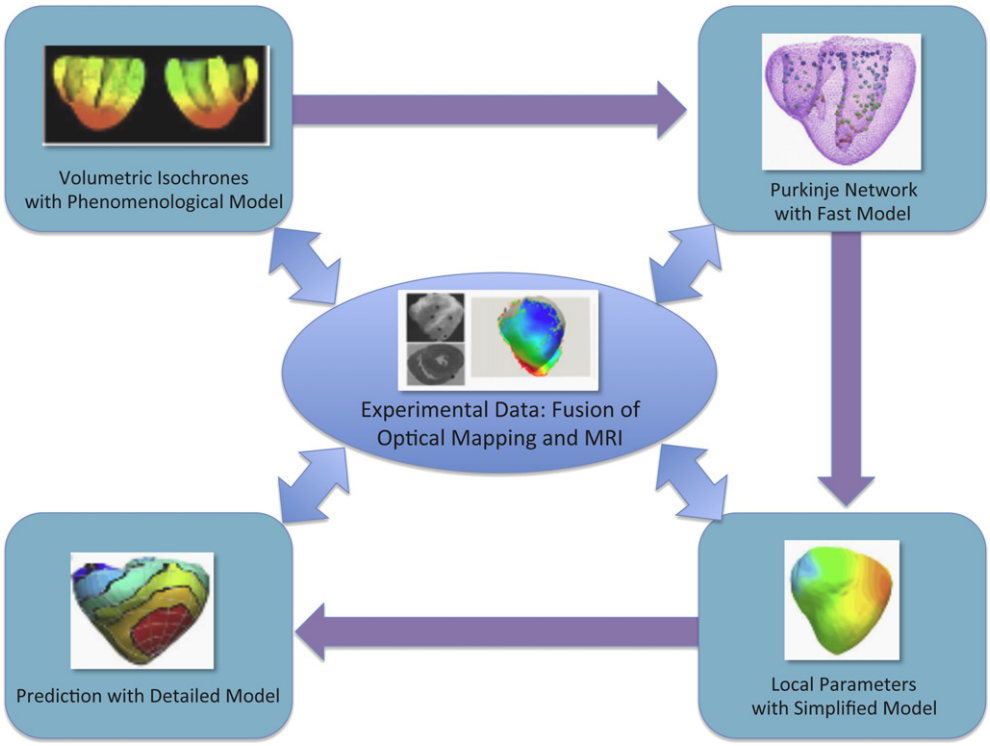

Fig. 1. Global scheme of the joint analysis and combination of the four different electrophysiological models with common experimental data.

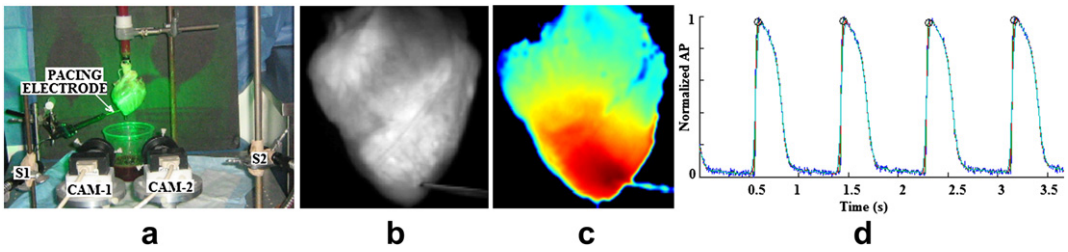

Fig. 2. Optical fluorescence imaging in explanted porcine heart perfused via a Langendorff system: (a) snapshot of the optical set-up using two CCD cameras; (b) 2D optical image showing the position of pacing electrode; (c) example of depolarization map record (red represents depolarization phase while blue represents repolarization phase); and (d) example of the normalized action potential waves recorded from one pixel at a pacing frequency of 1.1 Hz (shown over 3.7 s).

The main goal of this work is to present initial developments of an integrated system that combines these different model and personalization strategies. The proposed model pipeline propagates personalized material parameters and boundary conditions derived from simple models to customize more biophysically detailed models, as illustrated in Fig. 1 (velvet arrows indicate the order of the pipeline). This pipeline illustrates the complementary roles of statistical, phenomenological and biophysical approaches. Their common features and discrepancies are jointly analyzed when applying these models to assimilate the common experimental data (blue arrows in Fig. 1) and evaluate their observation reproducibility. The prediction capabilities of the integrated pipeline are assessed by estimating the activation time errors obtained in one pacing configuration with parameters learned in a different pacing scenario at every stage of the pipeline.

2. Experimental data and ground-truth

2.1. Optical mapping

Two swines weighting approximately 25 kg were anaesthetized, the chests opened, and their hearts exposed and excised after euthanasia (in accordance with animal research protocol guidelines approved at Sunnybrook Health Sciences Centre, Toronto, CA). The experiments are described in more detail in (Pop et al., 2009). Briefly, the aorta was rapidly cannulated and attached to a Langendorff perfusion system specially developed for explanted large hearts (see Fig. 2(a)). For the optical fluorescence imaging, a 20 mL bolus of fluorescence dye solution (di4-ANEPPS, Biotium Inc) was injected into the heart via the perfusion line. The voltage-sensitive dye was excited with green light (530 ± 20 nm) via 150 W halogen source lamps (MHF G150LR, Moritek Corp, Japan), labeled "S" in Fig. 2(a). The optical signals emitted from the hearts were filtered (>610 nm) and captured by two high-speed CCD cameras (MICAM02, BrainVision, Japan) at 270 frames/s. The field of view was 12×8 cm^2 yielding an approximately 0.7 mm spatial resolution.

Further analysis of the fluorescence signal (at each pixel) was performed in Matlab to study the action potential (AP) wave characteristics reflected by changes in fluorescence signal during depolarization and repolarization phases (see Fig. 2(c–d)). Next, the optical images recorded by the 2 CCD cameras were used to reconstruct a stereoscopic 3D surface of the heart, as described in (Chung et al., 2006). Furthermore, at the completion of the fluorescence recordings, several opaque markers were glued onto the epicardium and used for registering the 3D stereo surface to the volumetric mesh of the heart generated from MR images as explained in (Pop et al., 2007).

2.2. Magnetic resonance imaging and fusion with optical data

The hearts were gently placed in formalin and no longer than 3–4 days days later (to allow preservation of ventricle while avoiding further shrinkage), the surgically prepared ventricles were imaged using a 1.5-T Signa GE MR scanner for characterization of anatomy and myocardial fiber directions. The heart anatomy was extracted from the un-weighted images and used to generate the volumetric mesh for the mathematical models. The in-plane resolution was 0.5×0.5 mm^2 and slice thickness was 1.5 mm, which was suitable for the extraction of fibre direction and generation of high-quality meshes needed in multi-scale modelling.

The features computed from the optical data (depolarisation and repolarisation time isochrones) were projected on the volumetric myocardial mesh derived from the diffusion tensor MRI (DT-MRI) as detailed in (Pop et al., 2009). Here, we used one of the two available *ex-vivo* hearts, which were MR and optically imaged for steady state cycles, as illustrated in Fig. 2. The dataset we used contained 2 different optical datasets, paced at a frequency of 1.1 Hz, but obtained using 2 different pacing locations, near the apex of the Right Ventricle Epicardium (RV-Epi) and the Left Ventricle Endocardium (LV-Endo).

3. Personalization strategies for multi-level computational models of the heart

Four different computational models and personalization strategies were applied to the experimental data described above, each of these models having different levels of complexity and set of parameters:

1. Personalization of Purkinje terminals of the cardiac conduction system with an Eikonal method (PURK)
2. *Maximum a posteriori* estimation of 3D transmembrane potential using a simple phenomenological model as constraint (MAP)
3. A simplified reaction-diffusion electrophysiological 3D model (Mitchell–Schaeffer) with personalized tissue conductivity (MS)
4. A detailed biophysical ionic model with generic tissue conductivity parameters on a regularized heart shape and fibre orientation (IM)

3.1. Personalization of Purkinje terminals of the cardiac conduction system

There are some parameters that currently cannot be measured in vivo such as Purkinje fibre anatomy, which have a strong influence on the electromechanical behaviour of the heart (Romero et al., 2010). Zimmerman et al. (2009) developed a methodology to generate Purkinje trees specific to a given biventricular geometry. However, several parameters of the Purkinje tree generation such as the density of end terminals were not personalized and were chosen according to literature.

Camara et al. (2010b) recently presented a pipeline for the personalization of model-based Purkinje system using fast electrophysiological models and the optical mapping data described in Section 2. The regional density of the Purkinje terminals and the latest endocardial activation time were the parameters to personalize to better fit the available data. A genetic algorithm maximizing the similarity between the outcome of the electrophysiological simulations and measurements obtained from optical mapping data was used for the optimization of the parameters. Subsequently, the regional density of Purkinje terminals was then used to randomly distribute the stimulation points in each region. Finally, a Purkinje tree with 1D elements was constructed from the terminals following the shortest geodesic path principle to connect them to the main branching points (atrio-ventricular node, right and left bundle branching) that are manually defined (Pashaei et al., 2011). We also introduced into the personalization procedure the last activated endocardial stimulus since the available experimental data had a very long total activation.

In this paper, we used a simplified electrical wave propagation model that is solved on the *ex-vivo* porcine anatomical model, including the myocardial fibre orientation provided by the available DTI data and the Purkinje terminals given by the algorithm described above. The model that is used in this study is based on the Hamilton–Jacobi (HJ) equation. The Eikonal equation is an important member of the HJ equations, which can be described in anisotropic format as:

$$\begin{cases} \nabla\phi\mathbf{T}\mathbf{T}^T\nabla\phi^T - 1 = 0, & x_i \in \Omega \\ \phi(x_i) = \phi_0(x_i), & x_i \in \partial\Omega \end{cases} \quad (1)$$

where $\phi(x_i)$ is the activation time at the node i with position x_i, Ω is the myocardial computational domain and $\partial\Omega$ are the points containing initial values (stimulation points). $\mathbf{T}$ is the anisotropy tensor defined as $\mathbf{T} = \mathbf{AF}$, where $\mathbf{A}$ is the orthogonal matrix representing the unit vectors along the myofiber local coordinate system and $\mathbf{F}$ is a diagonal matrix whose diagonal elements are equal to the components of the conduction velocities along the myofiber local coordinate axes.

In order to solve this equation, we used the Fast Marching Method (Sethian, 1996) to Hamilton–Jacobi equations of Eikonal type by a finite difference discretization up-wind scheme. Simulations were performed using the OpenCMISS[2] numerical modelling environment. The conduction velocities along and transverse to the myocardial fibres were set to values from the literature (Caldwell et al., 2009). Hence, a value of 0.67 m/s was taken as conduction velocity along the myofibre axis and 0.24 m/s transverse to this, which was an average between the maximum conduction velocities parallel to the myocyte layers, 0.30 m/s, and normal to them, 0.17 m/s. These values resulted on an anisotropic ratio of conduction velocities equal to 2.8 between the longitudinal and transverse components. The conduction velocity of the Purkinje system was computed from the distance between the stimulus and the point with the latest endocardial time found in the optimization stage. One forward simulation of the Eikonal model took in average 5 s in a standard PC.

The cost function was the absolute mean error, integrated over all regions with available measurements, between simulated depolarization time maps and the ones extracted from the optical mapping data. Due to the discrete nature of the parameters to optimize and the randomness of the location of a particular Purkinje end-terminal within a region, we choose to use a classical genetic algorithm for the personalization of regional density of Purkinje end-terminals and for the latest endocardial time. Following observations by Durrer et al. (1970), we did not allow the presence of Purkinje end-terminals in some regions (mainly basal regions) and we forced the presence of at least one end-terminal in the remaining regions. The optimization of the Purkinje parameters with the genetic algorithm was quite demanding computationally due to the number of simulations per iteration. For convergence, 230 k simulations were run, taking around 10 h using 4 nodes of a cluster with 8 processors each. Details about the optimization algorithm can be found in Camara et al. (2010b).

3.2. Maximum a posteriori estimation of 3D transmembrane potential

To infer transmural electrophysiological details from surface mapping data is complicated due to the issue of model identifiability given limited quantity and quality of available observations. Therefore, simplified macroscopic PM models suit better this purpose with lower degrees of freedom and simplified description of tissue-level phenomena compared to cellular models. However, a simplified PM model introduces modeling errors not only in the parameters but also in the substantially simplified structures, plus other uncertainties coming from unknown initial conditions. It is thus challenging to attribute all these uncertainties to model parameters; especially when model parameters are optimized to fit one particular observation.

Hence Wang et al. (2010b) present the approach of Bayesian *maximum a posteriori* estimation that was originally developed to use non-invasive body-surface electrocardiographic data. Here this technique was adapted to use the provided epicardial optical mapping data described in Section 2 to estimate subject-specific volumetric transmembrane potential (TMP) dynamics. The ventricles are modelled by 1045 unconnected and meshfree points evenly-distributed inside the provided finite element mesh, where the fiber orientation of each point is interpolated from its nearest neighbour in the FEM mesh. The simple PM two-variable Aliev–Panfilov model (Aliev and Panfilov, 1996) is used to constrain the TMP estimation:

$$\begin{cases} \partial_t u = div(D\nabla u) + ku(u-a)(1-u) - uv \\ \partial_t v = -e(v + ku(u-a-1)) \end{cases} \quad (2)$$

where u is the normalized TMP and v the recovery current. The longitudinal and transverse components of the diffusion tensor D is set to 4.0 and 1.0 (Rogers and McCulloch, 1994), respectively. Parameters e, k and a determine individual TMP shapes, and here e and k are fixed to 0.01 and 8 (Aliev and Panfilov, 1996), respectively, setting a to 0.15 in TMP estimation and set to be unknown in dual TMP-parameter estimation. A mesh-free algorithm (Liu, 2003) is used to develop the model on the personalized heart structure and the Runge-Kutta method is used for implicit temporal discretization with adaptive resolution to support successful electrical propagation in relatively coarse spatial resolution. Unknown TMP associated with each point in the ventricles constitutes the state space in the estimation problem. One simulation with the Aliev–Panfilov model took around 4 min in average in a standard Macintosh.

From the filtered optical mapping data on the reconstructed stereoscopic surface, valid TMP signals were projected to the nearest 240 mesh-free points on the epicardial surface to constitute the data space in the estimation problem. The observation process is a straightforward, partial mapping from the state space of 3D ventricular mass (1045 meshfree nodes) to the data space of a fraction of epicardial surface (a subset of 240 meshfree nodes). The input optical mapping sequences are temporally scaled and interpolated to that of the model (2).

The estimation is performed in a statistical formulation to consider the effect of modeling error caused by parameters, structures and initial conditions and to couple a priori model and

[2] http://www.opencmiss.org.

personal data with respect to their uncertainties. First, the original physiological model is transformed and discretized into a stochastic state-space representation. MAP estimation is then performed based on the Unscented Kalman filter (Julier and Uhlmann, 1997) to preserve the non-linear dynamics and to accomodate the large-scale and high-dimensional nature of the system. Model and data uncertainty were assumed to be zero-mean Gaussian noises with predefined covariance matrices. Involving Monte-Carlo simulations of Aliev–Panfilov model, the MAP estimation of volumetric TMP engaged high computational times in the order of 250 hrs (~10 days). The interested reader is referred to (Wang et al., 2010a) for algorithmic details.

3.3. Simplified reaction-diffusion electrophysiological 3D model with local personalized parameters

Simple biophysical models (Bernus et al., 2002; Mitchell and Schaeffer, 2003; Bueno-Orovio et al., 2008) can describe and capture the shape of the cellular action potential and the propagation of the electrical wave, without modelling all ionic currents. These models offer a good compromise between the complexity and detail of the precise ionic models and the simple Eikonal-based wave propagation methods. Hence, Relan et al. (2010a,b, in press) presented the personalization of a subset of the Mitchell–Schaeffer model (Mitchell and Schaeffer, 2003) parameters with the optical mapping data described above. The MS model is quite convenient for this personalization framework since it has a limited number of parameters to estimate and each one has a simple interpretation. It also provides explicit analytical formulae to express most of the measured features and restitution properties using model parameters.

The MS model (Mitchell and Schaeffer, 2003) is described by the following system of Partial Differential Equations:

$$\begin{cases} \partial_t u = div(D\nabla u) + \dfrac{vu^2(1-u)}{\tau_{in}} - \dfrac{u}{\tau_{out}} + J_{stim}(t) \\ \partial_t v = \begin{cases} \dfrac{(1-v)}{\tau_{open}} & \text{if } v < v_{gate} \\ \dfrac{-v}{\tau_{close}} & \text{if } v > v_{gate} \end{cases} \end{cases} \quad (3)$$

where u is the normalised transmembrane potential variable, and v is a gating variable. The diffusion term in the model is controlled by the diffusion tensor D. This spatial diffusion can be related to a pseudo-conductivity of the cardiac tissue. In the longitudinal direction of the fibre, this pseudo-conductivity is set to a parameter d and to $d/2.5^2$ in the transverse directions (Keener and Sneyd, 1998). The MS model is spatially integrated using a linear tetrahedral mesh of the biventricular myocardium, that includes the fibre orientation provided by the available data, and is temporally integrated using an optimum time integration scheme (MCNAB), which was tested in details in (Ethier and Bourgault, 2008; Relan et al., 2009). One forward simulation of the MS model usually took around 20 min in average in a standard PC.

In this work, the personalization is performed by optimising the 3D model parameter representing the tissue conductivity based on the isochrones derived from the 2D epicardial surface data detailed in Section 2. Estimation of the tissue conductivity parameter is achieved using an iterative multi-resolution technique. We summarize here the approach, the details can be found in Relan et al. (2010a,b, in press). The estimation of the parameter d is achieved in two steps as follows:

- Calibration: used to initialise the parameters of the model. It is based on an analytical relationship between the conduction velocity and the diffusion parameter. It allows determining the initial parameter value d of each zone, using the median value of the conduction velocity computed from the actual data of this zone;
- Iterative adjustment: used to optimise the parameter d locally in space, using a multi-resolution technique, from the previous calibration result as an initial guess. The algorithm used here is a trust region method (Conn et al., 2000). In order to avoid piecewise constant parameter maps, we use a diffusive parameter regularisation at each iteration.

Parameter estimation of the diffusion parameters required computational times around 10 h for convergence.

3.4. Detailed biophysical model with generic parameters

If cardiac models are to be developed based solely on non-invasive diagnostic modalities, then a method for defining the myocardial conductivities is required. It is possible that aspects of cardiac physiology are either consistent within a pathology or, while significantly altered by disease, only have a limited impact on the sensitivity of model predictions of clinical relevant indices. Specifically if myocardial conductivity does not change significantly across a specific class of cardiac diseases, compared with, for example, heart geometry scaring or failure of the Purkinje network, then it is possible that using generic conductivity tensors derived from animal or human measurements may enable a sufficient representation of cardiac conductance to allow the simulation of realistic activation patterns.

Lamata et al. (2010b) investigated how detailed biophysical models could predict the experimental data described in Section 2 using generic conduction parameters taken from the literature. Therefore, three sets of bi-domain conductivities with different anisotropy ratios were taken from (Roth, 1997). For the joint analysis and the proposed integrated pipeline presented in this paper, the set of conductivities closer to the ones used by the other models was chosen, in this case with an anisotropy ratio of 2.75 between the longitudinal and transverse components of the conduction velocities. The isochrones of depolarization were then generated from simulations and compared to the experimental data.

We did not have access to a porcine cardiac electrophysiological model (none of the 252 models published on the CellML website[3] were labelled as porcine). Therefore, a human cell model, the ten Tusscher-Panfilov (TNNP) model (ten Tusscher and Panfilov, 2006), was used in all simulations. This was expected to have a nominal impact on activation times as both pigs and human have comparable conduction velocities (Caldwell et al., 2009) and maximum action potential upstroke rates (Pron et al., 2000). Simulations were performed using the CARP implementation of the mono-domain equations (Vigmond et al., 2003). A forward simulation of this ionic model usually took around 40 min in a high-performance cluster (an HPC with 128 cores) with a parallel implementation.

High resolution meshes are required for the simulation of these detailed models of cardiac electrophysiology, where a small spatial scale is necessary to capture the high spatial gradients. Therefore, we used an automatic modelling pipeline for the customization of corresponding mechanical (using 168 cubic Hermite elements) and electrophysiological (~65 million linear tetrahedra) meshes. This anatomical personalization uses medical image registration techniques to warp an idealized template (Lamata et al., 2010a), and regularizes both the heart shape and fibre orientation.

[3] http://www.cellml.org.

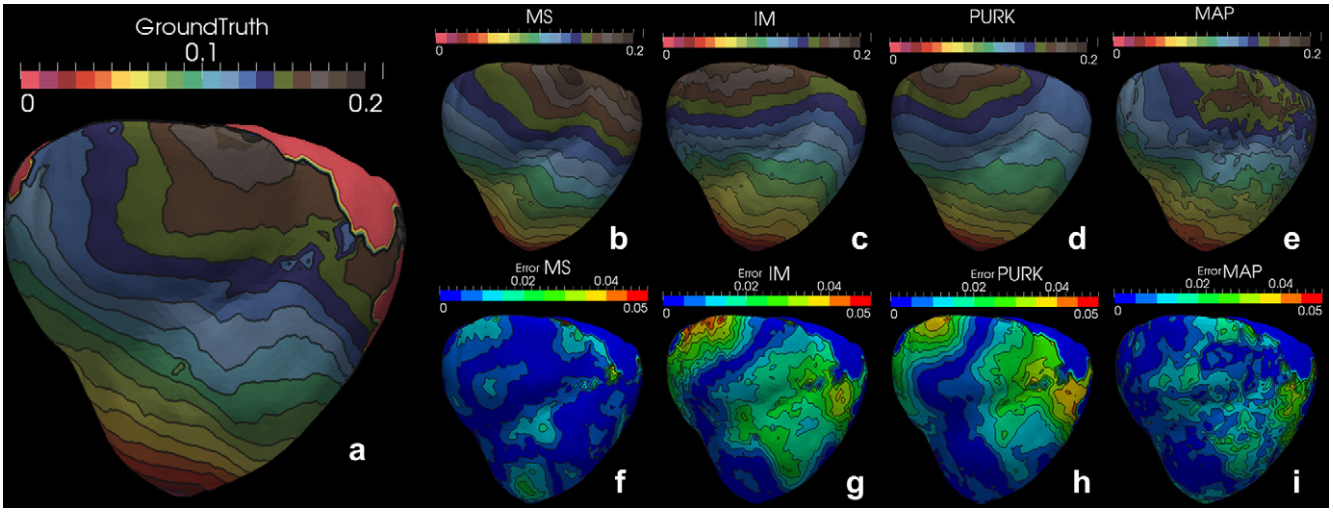

Fig. 3. Electrical activation isochrones provided by different models (from (b) to (e), MS, IM, PURK and MAP, respectively) and associated fitting error (from f) to i), MS, IM, PURK and MAP, respectively) with respect to the ground-truth given by optical mapping data with LV pacing (a). Units are in seconds.

4. Inter-model consistency and joint analysis

The computational models presented in the previous section are different representations of the same heart. Therefore, the joint analysis of results provided by these models can lead to a more complete understanding of their behaviour, which is fundamental for an optimal combination into an integrative pipeline. This allows the identification of differences between personalized models and association of these differences to particular characteristics and parameters of each model, which, in turn provides a platform for improvement and combination of their respective advantages. In this section, we present an inter-model verification where the four computational models described above are jointly analyzed.

The joint analysis performed in this work is focused on surface regions with available 2D optical mapping data. We computed the fitting errors between local depolarization times given by each computational model and the ones extracted from surface experimental isochrones. These fitting errors were studied regionally making use of the AHA segments (in this work, 26 regions, the classical 17 segments of the left ventricle (LV) and 9 additional segments for the right ventricle (RV)), classifying them into basal, mid and apical groups for each ventricle.

Fig. 3 shows the electrical activation isochrones provided by different models (from (b) to (e) in the figure) and the associated errors (from (f) to (i) in the figure) with respect to the ground-truth derived from optical mapping data (pacing at LV endocardium) at some parts of the epicardium ((a) in the figure). In a more quantitative way, Table 1 lists the corresponding regional mean local activation and total activation time (TAT) errors of the different models with respect to the ground-truth.

From a first visual inspection of the results shown in Fig. 3, it can be observed that the MS model ((b) in the figure) provides the closest isochrones to the ground-truth, which is also reflected in large areas of low errors in the corresponding error map (Fig. 3(f)) in areas of high and low conduction velocity. This fact can also be verified quantitatively in Table 1, where the MS model also presents the lowest global error for the whole heart (6.9 ± 3.1 ms). In general, IM and PURK models (Fig. 3(c) and (d), respectively) have more similar isochrone morphology between them compared to ground-truth or MS isochrones, in particular at the LV and RV basal segments, where they show larger differences in the associated error maps (large green areas, with some red spots indicating the largest errors in Fig. 3, (g) and (h) for IM and PURK models, respectively). This is also confirmed by quantitative general errors for the whole heart displayed in Table 1, which are substantially larger than MS model ones (16.2 ± 9.4 ms and 14.0 ± 7.8 for IM and PURK models, respectively). The MAP model, solving the problem from another point of view that does not fit model parameters but produces a probablistic estimation based on certain assumptions of model and data uncertainty, gives a fitting error in between (11.0 ± 6.0 ms).

Another global index for comparing simulation results and ground-truth is the total activation time (TAT) given by each electrical activation map where ground-truth is available. Using this index, the PURK and MAP models achieve a more similar TAT to the ground-truth (169.84 ms, 172.32 ms and 174.08 ms for ground-truth, PURK and MAP models, respectively), compared to the other models (193.41 ms and 181.72 ms for MS and IM models, respectively), as reported in Table 1. The incorporation of the fast conduction system into the PURK model with an optimized latest endocardial activation time to better fit the available data is probably the reason for the shortest TAT comparing to other models. Both MAP and PURK estimation procedures introduce an effect at the endocardium, that will activate faster than the rest of tissue, decreasing the TAT. On the other hand, the MS model provided the largest difference in TAT with respect to the ground-truth. Prospective visual inspection of the latest activated region in the available ground-truth data revealed the possibility of having data acquisition artifacts in this area that could mislead this TAT joint analysis.

Table 1
Regional (b: basal, m: mid, a: apical) and whole heart local depolarisation time as well as Total depolarisation time (TAT) errors where optical mapping measurements are available. Mean and standard deviation of absolute errors together with difference of the means (mean ± std/diff-mean) are provided for regions. Errors are reported in ms.

	MS	IM	PURK	MAP
LV b	$12.5 \pm 4.4/-10.5$	$19.3 \pm 2.0/16.9$	$28.2 \pm 0.9/28.1$	$20.3 \pm 10.3/17.2$
LV m	$7.9 \pm 2.9/6.1$	$16.9 \pm 4.0/16.6$	$12.8 \pm 5.3/12.5$	$13.9 \pm 3.6/13.6$
LV a	$6.3 \pm 2.1/-1.5$	$6.0 \pm 3.2/4.4$	$5.0 \pm 0.9/0.1$	$7.6 \pm 3.7/-0.7$
RV b	$5.9 \pm 1.3/-3.5$	$27.2 \pm 13.7/-18.1$	$19.5 \pm 1.1/-7.4$	$11.6 \pm 6.4/11.2$
RV m	$4.5 \pm 1.6/0.4$	$17.7 \pm 8.2/-10.7$	$14.2 \pm 5.2/-12.1$	$7.6 \pm 2.4/6.4$
RV a	$6.1 \pm 0/-1.7$	$9.5 \pm 0/-5.8$	$9.8 \pm 0/-9.9$	$5.8 \pm 0/5.1$
Whole	6.9 ± 3.1	16.2 ± 9.4	14.0 ± 7.8	11.0 ± 6.0
TAT	23.6	11.9	2.5	4.2

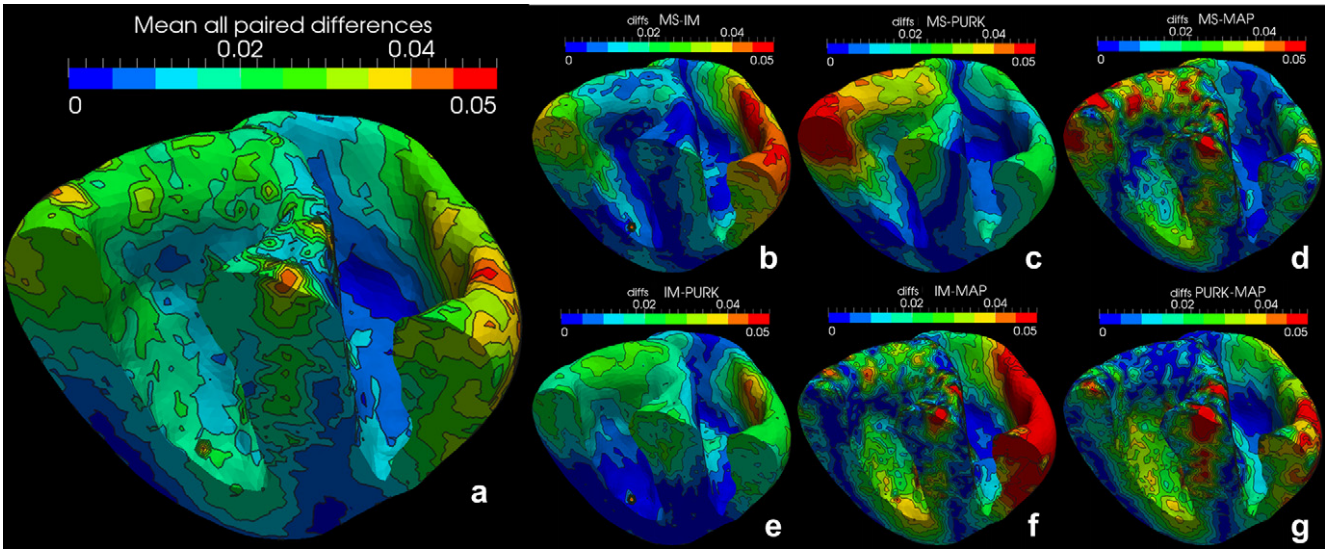

Fig. 4. (a) Mean of the differences between each pair of models at every node of the mesh; (b) to (e) Differences between every pair of simulation results. Units are in seconds.

In both models with personalized conduction parameters (MS) and MAP estimation (MAP), the largest errors occur in LV basal and middle regions. This indicates that the available optical mapping data at these regions poses the most significant challenges for different data assimilation strategies. This is likely because the data are most significantly different from a priori knowledge in these regions with respect to variations of conduction velocity. In models with personalized Purkinje network (PURK) or specific fibre structure (IM) but with generic conductivity parameters, the largest errors occur in RV basal regions in addition to LV basal regions; RV middle regions also exhibit relatively large errors compared to the other regions. In the RV and LV free walls, the experimental data showed a faster and slower conduction, respectively, that IM and PURK models were unable to capture, probably due to the model assumptions of healthy tissue on the different conduction parameters (homogeneous conductivity and ion channel dynamics across the membrane). MAP estimation exhibits relatively large errors in LV apical region compared with the other methods as well as with MAP estimation of the other regions. The reason for this error is that the TMP estimation did not utilize the pacing location as prior knowledge to initialize the constraining model, thus this erroneous initial condition has to be corrected by the optical mapping data. In this case, as the LV apical region is the first excited region due to pacing, optical mapping data information comes available at the early stage of the time sequence, which is most likely happening before the convergence of the estimation algorithm. Also note that, owing to the prediction-correction mechanism, the MAP estimation also exhibits a higher level of noise compared to the other models.

Finally, we also analyzed the differences between each pair of models as well as their mean, as illustrated in Fig. 4. It needs to be pointed out that these differences also give information transmurally, not just in the 2D surfaces were experimental data was available. Fig. 4 shows that there are clear discrepancies between the model predictions of activation time, primarily at the base of both ventricles, compared with the similarities between predictions at the apex. For instance, largest paired differences (red in Fig. 4) appeared in basal LV and RV free walls. This was expected since the pacing point was located at the LV apical endocardium.

We can also notice that differences were larger on thicker walls (e.g., RV free wall in Fig. 4(b) and (f), or LV free wall in (c)), where a larger intramural propagation is needed. On the other hand, endocardial regions corresponding to thinner walls present small differences. Once the epicardium ground-truth data is assimilated into the models, there are small differences between different simulation results where ground-truth data is available. Subsequently, if the electrical wave is propagated through thin walls to the endocardium, there is not enough tissue for the different models to diverge that, in contrast, happens in the case of thicker walls at the farthest points from the ground-truth.

5. Complementarity between different multi-level computational models

5.1. Proposed approach to integrate the different models

In this section we tried to combine the specificity of each model in order to integrate the different personalization strategies for prediction. Based on the analysis of the strengths and possible input–output of each method, we chose a coarse-to-fine strategy where the simpler models are firstly personalized with the available data and the resulting parameters are integrated as personalized parameters (or data) for the following stages. This coarse-to-fine approach, using

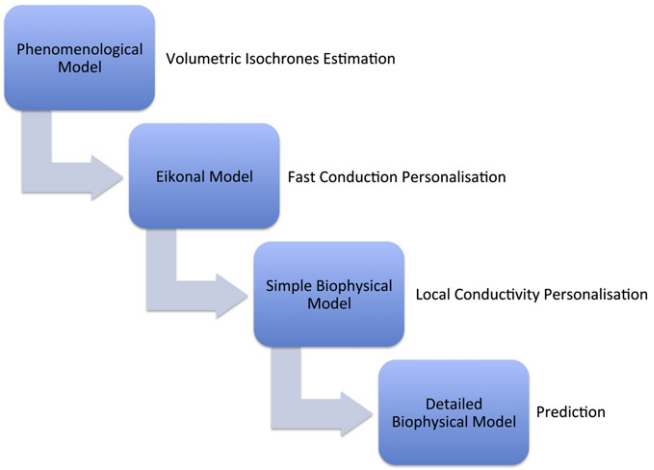

Fig. 5. Proposed simulation pipeline combining the different models and their personalisation.

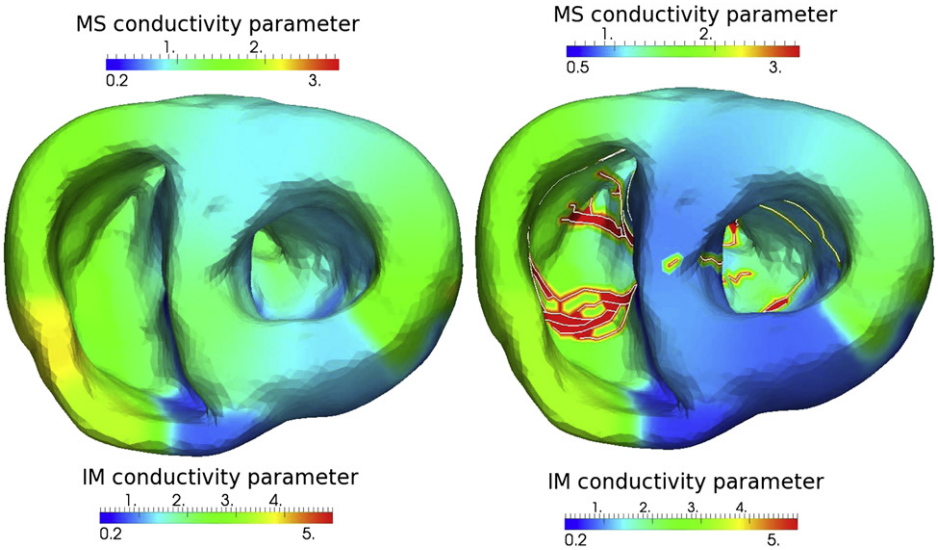

Fig. 6. Personalization of conductivity/diffusion parameters. Left: Diffusion map without considering the Purkinje system. Right: Diffusion map with the Purkinje system.

simpler and faster models first and finally the more detailed ones aims at avoiding the curse of dimensionality (see (Garny et al., 2005)) and at achieving reasonable computational time. The proposed approach can be split into the following steps (see Fig. 5):

1. Probabilistic state estimation to obtain regularised and volumetric isochrones
2. Eikonal model to personalize the fast cardiac conduction system
3. Phenomenological model to personalize local conductivity/diffusion parameters
4. Detailed ionic model to test personalized prediction

The first stage is the MAP state estimation to generate volumetric isochrones considering a simple model and incomplete data uncertainties from the available 2D optical measurements at the epicardium. Subsequently, the optimization of the Purkinje tree with a fast electrophysiological model based on Eikonal equation, is applied to personalize the fast conduction system. The following step uses the Purkinje tree resulting from the previous phase to initialize the personalization of conductivity/diffusion parameters of a simple phenomenological model. Fig. 6 shows the obtained diffusion maps after the personalization stage without and with considering Purkinje (left and right in the figure, respectively). These personalized parameter maps are then incorporated into a detailed generic biophysical model as boundary conditions. This last step provides the most personalized and complete simulation results. It combines personalized parameters extracted with the simplest models, which were embedded in an optimization procedure with reasonable computational costs, together with a detailed IM.

5.2. Integration methodology

Some practical considerations were required in order to combine the different approaches:

1. Firstly, the mesh-free estimation of TMP throughout the myocardium was achieved as in the previous section. The results were interpolated on the original mesh.
2. The resulting volumetric isochrones were then used by the Purkinje tree estimation instead of the original surface ones for the personalization of the fast conduction system. The idea is that the interpolation provided by the first step can help in the convergence of the Purkinje tree estimation
3. This personalized Purkinje tree was introduced in the simple phenomenological model personalization by setting a high conductivity to the tetrahedra containing this tree. Thus a fast conduction network was present in the simple phenomenological model.
4. Subsequently, a calibration was performed between the simple phenomenological and the detailed biophysical models in order to find a mapping between the diffusion parameter in each model. Finally, the obtained conductivity per tetrahedron estimated with the simple phenomenological model was interpolated on the mesh used by the detailed model.

As the different reaction-diffusion models are based on different equations, different discretisation methods and different mesh

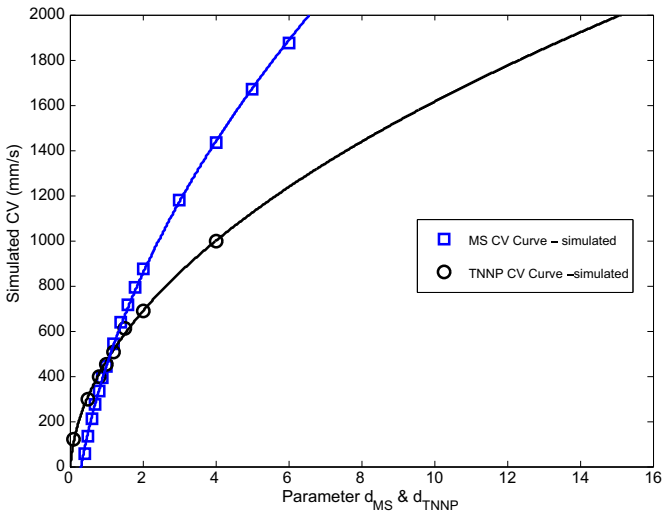

Fig. 7. Calibration between the different model diffusion/conductivity parameters. Each dot represents the average conduction velocity for a simulation with a given D value for the MS (blue) and a scaling factor of the TNNP (black) model conductivity parameters.

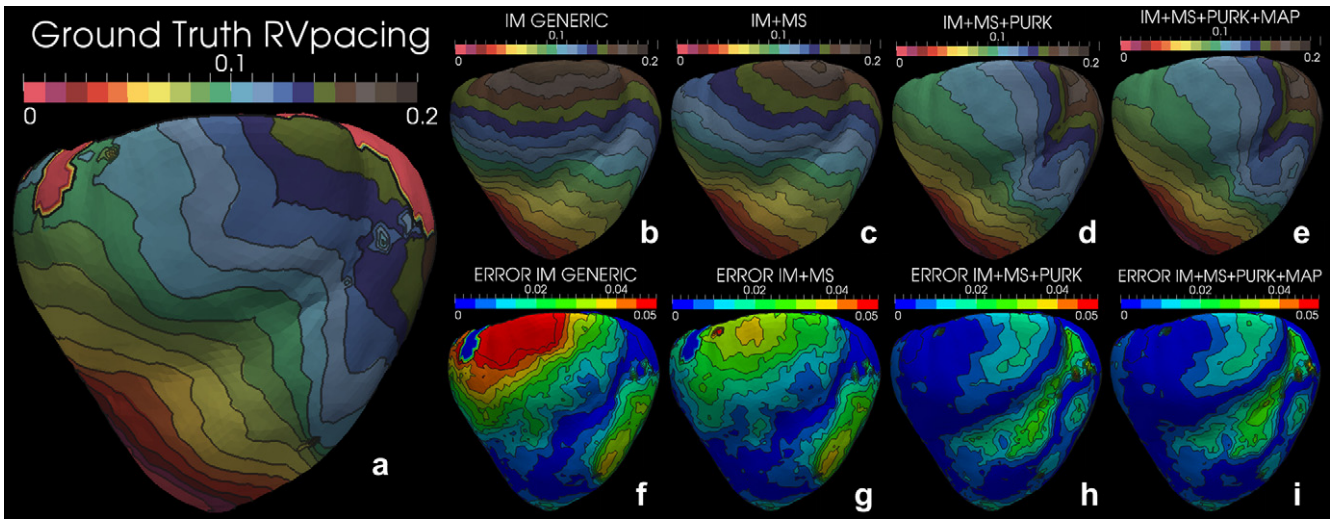

Fig. 8. Electrical activation isochrones obtained at different stages of the proposed pipeline (from (b) to (e), IM generic, IM + MS, IM + MS + PURK and IM + MS + PURK + MAP, respectively) and associated prediction error (from (f) to (i), M generic, IM + MS, IM + MS + PURK and IM + MS + PURK + MAP, respectively) with respect to the ground-truth given by optical mapping data with RV pacing (a). Units are in seconds.

resolutions, trying to analytically relate the parameters would be difficult, and would anyway not give the same numerical results. Indeed, the approximation errors are different, thus it would not lead to a direct link between the different implementations. Therefore, we designed an alternative strategy that relies on a calibration of conductivity parameters between the different models in order to re-use the parameters estimated with one model for simulations based on a different model. There is a known quadratic functional relationship between diffusion/conductivity parameters, D, and the velocity of propagation of the depolarisation wave or conduction velocity, CV : $CV \propto \sqrt{D}$. Hence, simulations of each model were run for a range of D values on the same heart geometry (from the experimental data), to find the corresponding conduction velocities (see Fig. 7). A square-root function was fitted to these values, and the mapping to transfer D values from one model to the other was computed. Details on this mapping can be found in Relan et al. (2010a,b), where a similar coupling strategy was used between the Eikonal and the MS models. After this calibration, the different models do provide similar values in terms of depolarisation times due to this agreement between them, up to this calibration scaling. The scaling between the MS and the IM models can be appreciated in the colour legend for the diffusion maps shown in Fig. 7.

5.3. Predictive value of integrated computational models

The evaluation of the integrated approach is based on a prediction scenario, where the parameters learned in a pacing condition (LV endocardial stimulation protocol analyzed in Section 4) are used to estimate the depolarization isochrones in a different pacing scenario (RV epicardial stimulation condition). The predictive value is evaluated by the differences in time of activation between model results and experimental data in the epicardial region where ground truth is available. Each step of the coarse-to-fine model concatenation is evaluated separately, and results are presented in Fig. 8. From an initial inspection of Fig. 8 it is straightforward to identify the reduction of errors when incorporating personalized information from the MS model into the IM model with generic parameters (Fig. 8(f) and (g), respectively). Furthermore, it can also be observed the positive effect of incorporating the personalized Purkinje tree into the pipeline (Fig. 8(d)), making activation propagation direction more similar to the data to predict. Finally, the incorporation of the MAP estimation does not seem to substantially change prediction performance of the pipeline. In a more quantitative way, prediction errors (mean ± standard deviation) averaged over the whole heart in each step of the pipeline confirm observations from the figure: IM generic, 17.95 ± 13.10 ms; IM + MS, 13.45 ± 8.52 ms; IM + MS + PURK, 10.09 ± 6.27 ms; IM + MS + PURK + MAP, 10.46 ± 6.75 ms. For comparison, prediction errors obtained with the MS and PURK methods run individually were computed: MS, 11.62 ± 9.25 ms; PURK, 18.16 ± 11.46 ms. We did not include the MAP method in this prediction scenario since it is basically an extrapolation method balancing measurements an electrophysiological model to cope with both parameter and data uncertainties.

6. Discussion and conclusions

The integration of different personalized models of cardiac electrophysiology for prediction purposes involves the critical issue of identifiability and uniqueness of parameters given limited measurements, as well as the intricate, non-linear relationship between most parameters and the measurements. The complexity of cardiac electrophysiology makes these questions mathematically formidable, if not intractable. This paper intends to initiate a first effort into this direction with a pipeline integrating different modelling methods that improves the prediction of depolarization isochrones.

Experimental data containing the cardiac anatomy and fibre orientations from MRI, as well as epicardial transmembrane potentials from optical mapping acquired on *ex-vivo* porcine hearts was used to generate ground-truth data for model assessment (see Section 2). The whole process of data acquisition and processing involved a number of operations that are potential sources of error that necessarily have an influence on the final ground-truth data. For instance, optical measurements do not really correspond to epicardial potentials but rather integrate the effect of a volume of tissue below the epicardium, which is dependent on the local orientation of the surface with respect to the light and camera settings. Correcting the simulated voltages as well as better interpretation of the optical upstroke shapes such as proposed by Hyatt et al.(Hyatt et al., 2005) and Bishop et al.(Bishop et al., 2006), could improve the quality of the correspondence between measurements and simulations. In addition, the available MRI spatial resolution

(1.5 mm slices) limits the extracted fibre orientation to be only a coarse representation of the microstructural complexity of the heart, particularly at areas with a high degree of orientation variability such as the apex. Regarding experimental data processing, some steps were needed to extract the depolarization times and compare them to simulations such as the 3D stereo reconstruction from the 2D optical mapping images and 3D MRI. This registration consisted on a rigid transformation between the optical and MR surfaces based on limited markers positions, with errors in marker's coordinates lower than 3 mm (Pop et al., 2009).

The experimental data from the LV endocardial pacing condition was reproduced by four distinct modelling approaches. An IM with generic parameters taken from the literature, with no personalization involved, obtained average errors of 16.2 ms. Estimation of the Purkinje system based on an Eikonal model, with 27 parameters, reduced the error to 14.0 ms, and a regional estimation of local conductivities with a PM, with 85 parameters, reached an error of 6.87 ms. Note that a MAP model does not fit parameters or aim to reproduce the data, and that its fitting error (11.0 ms) represents an estimation assuming the existence of uncertainties in both generic prior knowledge and input optical mapping data. Noting the Akaike information criterion (Akaike, 1974), it should be assessed if the improved accuracy with each of the different models is justified by the increased number of fitted parameters or complexity.

Reduction of fitting error with further complexity does not necessarily result in a better and more predictive model (e.g. overfitting of the parameters to a given dataset). Thus, the evaluation of the integrated pipeline was based on a predictive scenario, where two different pacing conditions were used: an LV endocardial pacing for parameter fitting; and an RV epicardial pacing for prediction once the model is personalized with the LV endocardial pacing. The obtained results demonstrate the gradual increase of predictive accuracy with increased model complexity (from 17.95 ± 13.10 ms with IM generic to 10.09 ± 6.27 ms with the 3-step pipeline). Nevertheless, the incorporation of a volumetric estimation of the TMP (4-step pipeline) did not enhance the predictive performance of the pipeline (10.46 ± 6.75 ms), even though this did change the estimation of the Purkinje system and the regional conductivities. When computing the prediction accuracy of individual models (MS, PURK, IM), the whole pipeline still gave the best prediction power. These observations shed valuable light on the inter-model consistency and complementarity, as well as the direction of pipeline development.

The coarse-to-fine strategy we have proposed for the integrative pipeline where simpler models and firstly personalized with the available data to initialize the more detailed models aims at achieving reasonable computational times and at avoiding the curse of dimensionality (Garny et al., 2005). Phenomenological models presented relatively small computational times that allowed them to be embedded in optimization procedures with large number of iterations. Nevertheless, it would be useful to compare this strategy with a multi-level optimization on the ionic models. With the increase of computational power, use of high-performance computing infrastructures and the optimal parallelization and scalability of the model implementations, ionic models would soon be ready for parameter optimization procedures (see (Niederer et al., 2011)), but there would still be present the issue of dimensionality. This dimensionality aspect is important in the personalization of models, because in addition to the computational time, there is also an increase in the number of model parameters which makes the question of the observability of these parameters from the data challenging.

First, having better performance with the 3-step pipeline than with the 4-step one might illustrate the redundant role of some parameters in different models (e.g. the Purkinje system in PURK and regional conductivities in other models) may have to represent the same physiological characteristics that affect the observed epicardial data. In other words, given partial, epicardial optical data, some modeling aspects of the heart might not be separable or uniquely identified in theory, increasing the difficulty of integration of several models. Therefore, even though two sets of parameters (diffusion and density of Purkinje terminals) are with different values in the 4-step pipeline and 3-step pipeline, their combination eventually leads to similar prediction power. The use of more complete ground-truth data (i.e. from contact or non-contact electro-anatomical mapping systems) including sinus rhythm, several pacing configurations (i.e. number and position of leads) and presence of scar would allow to better study the effect of Purkinje and conductivities in different physiological conditions.

The proposed simulation pipeline is developed following a heuristic approach, combining the optimization results sequentially. As observed above, the change of the optimized parameters in one step is compensated by the parameter optimization in the following steps, i.e. leading to the change in the subsequent parameters despite the overall similar prediction power of the pipeline. Theoretically, different parameters such as the Purkinje network plus different electrical properties of cells, tissue and model structures, should be personalized at the same time according to their respective impact on the measured data. This will ensure variations in model output to be correctly apportioned to different sources of variation in these parameters. Consequently, the non-uniqueness of Purkinje and conductivity parameters, as observed in our results, might not be caused by the theoretical identifiability issue, but owing to the heuristic approach proposed. Furthermore, as different components in the pipeline carry out the personalization independently using the same data, bias might be introduced in one component and passed on to the following components, leading to possible conflicts. Hence, the development of appropriate integrative personalization pipelines still remains a challenging task that requires thorough insights into the complementarity and consistency of the different parameter optimization approaches.

Lastly, it could also be argued that, even though the combination of parameters does not substantially change the prediction power in some stages of the pipeline (as shown in the 4-step and 3-step pipeline), the separate parameters might be drawn closer to their physiological validity because of the integration with other models. In other words, the proposed heuristic approach might be able to help apportion the variation in model output to the different parameters in the model. If the complete integrated representation of the heart is congruent with the different model used, this could be used as a surrogate of its physiological validity. Further investigation on the physiological validity of the individual parameters is needed. Furthermore, the very similar prediction performance of the 4-step pipeline and the 3-step pipeline also suggests that the possible noise in data, or the possible bias introduce by MAP, is compensated by the following modeling steps, which can be interpreted as a robustness of the pipeline. Further research is needed to investigate these limitations and advantages of the combination of modeling strategies.

The scope and validity of proposed pipeline is limited by several assumptions and methodological choices. The MAP model did not include any a priori knowledge of a Purkinje system or conductive heterogeneity, what is believed to bias the estimation of the parameters of this system in the subsequent steps. The Purkinje system is modelled as a concatenation of elements with very high conductivity, and, as such, it is always captured when any depolarization wave reaches it. In addition, optical measurements were only available at the epicardium while the Purkinje model was placed endocardially since we took a human heart configuration. An

alternative that could eventually improve data fitting would be to include transmural terminals such as in the pig heart, in particular if 3D optical data from the porcine heart were available. The regional estimation of parameters captures heterogeneities as a scale of the conductivity, regardless of any anisotropy of this parameter. This regional estimation is therefore done only at tissue level, with no personalization of the upstroke rate at the cellular level. Different anisotropy ratios between the longitudinal and transverse components of the conductivity parameters were used in the different models, within a reasonable range (2.0, 2.5, 2.75, 2.8). It would be convenient to homogenize these parameters, although some previous results suggest that the simulated activation patterns are not very sensitive to these anisotropy ratio small changes (Lamata et al., 2010b). Furthermore, different anatomical model representations of the data (hexahedral, coarse and fine tetrahedral meshes, mesh-free) were used by the different computational models of the proposed pipeline, thus interpolation errors might occur and accumulate in the pipeline. Future work will be focused on the optimal combination of models in a pipeline where the different methodological choices are better integrated including mesh compatibility, simultaneous parameter optimization, conductivity parameter value homogenization or use of volumetric ground-truth data.

The complexity of cardiac electrophysiology brings difficulties for an objective, comprehensive assessment of the quality of the prediction power of the proposed pipeline. In this paper, the accuracy of the prediction has mainly been evaluated by the total activation time error and by regional differences of activation. Future work will consider a more thorough analysis including the pattern, propagation direction, and repolarization properties of the simulated electrical activity. Furthermore, physiological validity of individual model parameters, such as the Purkinje system and regional tissue conductivities, in addition to the overall behavior of the model are essential for assessing the benefits brought in by the integrated pipeline.

As presented, models of four different levels of complexity were used for the purpose of a subject-specific electrophysiological understanding of the heart. This joint analysis shows that there is no unique answer as to the optimal level of model details to be used for improving our knowledge on heart physiology. When the data is limited in quantity and quality, as discussed above, and the prior knowledge of subject-specific conditions are scarce, MAP estimation appears to be a viable option. This is because the TMP phenomena (estimation target) have more direct relations to the observation data compared to other electrophysiological parameters and this method deals with errors in measurement data and standard simple models. However, as a result of the limited information being utilized, there is also a limit to the details and accuracy of electrophysiological information that could be delivered by MAP estimation. Namely, while it might be sufficient for certain diagnostic purposes (Wang et al., 2011), it cannot guarantee a high-resolution, scientifically-accurate subject-specific electrophysiological activity. Models of higher levels of detail would solve this problem, but as the level of detail increases and the parameters being personalized (such as Purkinje network, tissue conductivity, etc.) have less direct relations to the observation, the requirement on measurement data increases in order to ensure model parameter identifiability. These paradoxes may further justify the importance of the proposed effort in developing integrated pipelines that combine the advantages of different approaches to improve the overall electrophysiological understanding of the heart.

The final objective is to integrate the use of computational models into clinical routine, and validation is key to build the trust in these tools. In this work we have addressed one of the most desired modelling capabilities, its predictive power. Model concatenation has led to a reduction of prediction error. Nevertheless, quantitative experimental validation of the personalized electrophysiological models of the heart are by no means trivial, as it ideally requires a set of in vivo data including subject-specific anatomical geometry of the heart, its constituent structure that impacts electrical conduction including Purkinje network and fiber structure, its regional electrical activities and properties (e.g., conductivities) not only on heart surfaces but along the depth of the myocardium. The availability of this type of data is very limited, and therefore presents a challenge to translate these validation methodology and results into a clinical setting.

An integrated pipeline of cardiac electrophysiological models has demonstrated to increase the predictive power of depolarization isochrones. Results also suggest that this integrated approach could have important benefits, such as an improved robustness to noise or a higher physiological realism. Nevertheless, results also illustrate that further investigations are needed regarding the increase of model complexity and the parameter uniqueness and identifiability.

Editor's note

Please see also related communications in this issue by Clayton et al. (2011b) and Quinn et al. (2011).

Acknowledgments

Financial support for this work was provided by different organisations and projects: the Canadian Institutes of Health Research grant (MOP93531); the Networking Research Center on Bioengineering, Biomaterials and Nanomedicine (CIBER-BBN), the European Community's Seventh Framework Programme (FP7/2007-2013) under grant agreement n. 224495 (euHeart project); the CENIT Program from Spanish MICINN-CDTI under grant CEN20091044 (cvREMOD project); the United Kingdom Engineering and Physical Sciences Research Council through grants EP/F043929/1 and EP/F059361/1; the National Basic Research Program of China (No: 2010CB732500) and the National Natural Science Foundation of China(No: 60872068). OC acknowledges grant support from the Spanish Ministry of Research and Innovation under a Ramon y Cajal research fellowship. AFF holds an ICREA-Academica Prized from the Institució Catalana de Recerca i Estudis Avançats (ICREA). Technical support was provided by the Oxford Supercomputing Centre and HECToR (UK National Supercomputing Service) for the detailed simulations.

References

Akaike, H., 1974. A new look at the statistical model identification, automatic control. IEEE Trans. 19, 716–723.
Aliev, R.R., Panfilov, A.V., 1996. A simple two-variable model of cardiac excitation. Chaos Soliton Fract 7, 293–301.
Aliot, E., Stevenson, W., Almendral-Garrote, J., 2009. EHRA/HRS expert consensus on catheter ablation of ventricular arrhythmias. Europace 11, 771–817.
Bernus, O., Wilders, R., Zemlin, C., Verschelde, H., Panfilov, A., 2002. A computationally efficient electrophysiological model of human ventricular cells. Am. J. Physiol. Heart Circ. Physiol. 282 H2296.
Bishop, M., Rodriguez, B., Eason, J., Whiteley, J., Trayanova, N., Gavaghan, D., 2006. Synthesis of voltage-sensitive optical signals: application to panoramic optical mapping. Biophysical J. 90, 2938–2945.
Bueno-Orovio, A., Cherry, E., Fenton, F., 2008. Minimal model for human ventricular action potentials in tissue. J. Theor. Biol. 253, 544–560.
Caldwell, B., Trew, M., Sands, G., Hooks, D., LeGrice, I., Smaill, B., 2009. Three distinct directions of intramural activation reveal nonuniform side-to-side electrical coupling of ventricular myocytes. Circ. Arrhythm Electrophysiol. 2, 433–440.
Camara, O., Pop, M., Sermesant, M., Smith, N., Young, A., 2010a. Statistical Atlases and Computational Models of the Heart, first ed., 6364. Springer-Verlag, Berlin, Germany.
Camara, O., Pashaei, A., Sebastian, R., Frangi, A., 2010b. Personalization of fast conduction Purkinje system in Eikonal-based electrophysiological models with optical mapping data, in: International workshop on Statistical Atlases and

Computational Models of the Heart and Cardiac Electrophysiological Simulation Challenge (STACOM-CESC'10), LNCS 6364, pp. 281–290.
Camara, O., Riccobene, C., Romero, D., Pashaei, A., Sebastian, R., Sukno, F., Butakoff, C., De Craene, M., Omedas, P., Frangi, A.F., Velut, J., Philipot, C., Tomoulin, C., Billet, F., Mansi, T., Sermesant, M., Wallman, M., Rodriguez, B., Lamata, P., Smith, N., Chinchapatnam, P., Duckett, S., Razavi, R., Groth, A., Weese, J., Ecabert, O., 2010c. Patient-specific computational models of the heart for a cardiac resynchronization therapy planning platform, in: 1st International Conference on Virtual Physiological Human (VPH'10).
Chinchapatnam, P., Rhode, K., Ginks, M., Rinaldi, C., Lambiase, P., Razavi, R., Arridge, S., Sermesant, M., 2008. Model-based imaging of cardiac apparent conductivity and local conduction velocity for diagnosis and planning of therapy. IEEE Trans. Med. Imaging 27, 1631–1642.
Chung, D., Pop, M., Sermesant, M., Wright, G., 2006. Stereo reconstruction of the epicardium for optical fluorescence imaging, in: MICCAI Workshop on Biophotonics for diagnosis and treatment. Institute of Mathematical Modelling (IMM), Technical University of Denmark, Technical Report, pp. 33–40.
Clayton, R., Bernus, O., Cherry, E., Dierckx, H., Fenton, F., Mirabella, L., Panfilov, A., Sachse, F., Seemann, G., Zhang, H., 2011a. Models of cardiac tissue electrophysiology: progress, challenges and open questions. Prog. Biophys. Mol. Biol. 104, 22–48.
Clayton, R., Nash, M., Bradley, C., Panfilov, A., Paterson, D., Taggart, P., 2011b. Experiment-model interaction for analysis of epicardial activation during human ventricular fibrillation with global myocardial ischaemia. Prog Biophys Mol Biol. 107, 101–111.
Conn, A., Gould, N., Toint, P., 2000. Trust Region Methods. SIAM.
Durrer, D., van Dam, R.T., Freud, G.E., Janse, M.J., Meijler, F.L., Arzbaecher, R.C., 1970. Total excitation of the isolated human heart. Circulation 41, 899–912.
Ethier, M., Bourgault, Y., 2008. Semi-implicit time discretization schemes for the bidomain model. SIAM J. Numer. Anal. 46, 2443–2468.
Fink, M., Niederer, S.A., Cherry, E.M., Fenton, F.H., Koivumki, J.T., Seemann, G., Thul, R., Zhang, H., Sachse, F.B., Beard, D., Crampin, E.J., Smith, N.P., 2011. Cardiac cell modelling: observations from the heart of the cardiac physiome project. Prog. Biophys. Mol. Biol. 104, 2–21 (Cardiac Physiome project: Mathematical and Modelling Foundations).
Garny, A., Noble, D., Kohl, P., 2005. Dimensionality in cardiac modelling. Prog. Biophys. Mol. Biol. 87, 47–66.
Hyatt, C., Mironov, S., Vetter, F., Zemlin, C., Pertsov, A., 2005. Optical action potential upstroke morphology reveals near-surface transmural propagation direction. Circ. Res. 97, 277–284.
Julier, S.J., Uhlmann, J.K., 1997. A new extension of the Kalman filter to nonlinear systems, in: International Symposium on Aerospace/Defense Sensing, Simulation, and Controls, pp. 182–193.
Keener, J., Sneyd, J., 1998. Mathematical Physiology. Springer-Verlag, New York.
Lamata, P., Niederer, S., Barber, D., Nordsletten, D., Lee, J., Hose, R.D., Smith, N., 2010a. Personalization of cubic hermite meshes for efficient biomechanical simulations, in: Med Image Comput Comput Assist Interv (2), pp. 380–387.
Lamata, P., Niederer, S., Plank, G., Smith, N., 2010b. Generic conduction parameters for predicting activation waves in customised cardiac electrophysiology models, in: International workshop on Statistical Atlases and Computational Models of the Heart and Cardiac Electrophysiological Simulation Challenge (STACOM-CESC'10), LNCS 6364, pp. 261–269.
Liu, G., 2003. Meshfree Methods. CRC Press, Boca Raton, FL.
Mitchell, C.C., Schaeffer, D.G., 2003. A two current model for the dynamics of cardiac membrane. Bull. Math. Biol. 65, 767–793.
Niederer, S., Mitchell, L., Smith, N., Plank, G., 2011a. Simulation human cardiac electrophysiology on clinical time-scales. Front. Physiol. 2, 1–7.
Niederer, S.A., Plank, G., Chinchapatnam, P., Ginks, M., Lamata, P., Rhode, K.S., Rinaldi, C.A., Razavi, R., Smith, N.P., 2011b. Length-dependent tension in the failing heart and the efficacy of cardiac resynchronization therapy. Cardiovasc. Res. 89, 336–343.
Noble, D., 1962. A modification of the Hodgkin–Huxley equations applicable to Purkinje fibre action and pace-maker potentials. J. Physiol. 160, 317–352.
Pashaei, A., Hoogendoorn, C., Sebastián, R., Romero, D., Camara, O., Frangi, A.F., 2011. Effect of scar development on fast electrophysiological models of the human heart: In-silico study on atlas-based virtual populations, in: International Conference on Functional Imaging and Modeling of the Heart (FIMH'11), LNCS 6666, pp. 427–436.
Pop, M., Sermesant, M., Chung, D., Liu, G., McVeigh, E., Crystal, E., Wright, G., 2007. An experimental framework to validate 3D models of cardiac electrophysiology via optical imaging and MRI, in: Proceedings of Functional Imaging and Modeling of the Heart 2007 (FIMH'07), volume 4466 of LNCS, pp. 100–109.
Pop, M., Sermesant, M., Lepiller, D., Truong, M., McVeigh, E., Crystal, E., Dick, A., Delingette, H., Ayache, N., Wright, G., 2009. Fusion of optical imaging and MRI for the evaluation and adjustment of macroscopic models of cardiac electrophysiology: a feasibility study. Med. Image Anal. 13, 370–380.
Pron, Y., Demolombe, S., Bar, I., Drouin, E., Charpentier, F., Escande, D., 2000. Differential expression of kvlqt1 isoforms across the human ventricular wall. Am. J. Physiol. Heart Circ. Physiol. 278, H1908–H1915.
Quinn, T.A., Granite, S., Allessie, M.A., Antzelevitch, C., Bollensdorff, C., Bub, G., Burton, R.A., Cerbai, E., Chen, P.S., Delmar, M., Difrancesco, D., Earm, Y.E., Efimov, I.R., Egger, M., Entcheva, E., Fink, M., Fischmeister, R., Franz, M.R., Garny, A., Giles, W.R., Hannes, T., Harding, S.E., Hunter, P.J., Iribe, G., Jalife, J., Johnson, C.R., Kass, R.S., Kodama, I., Koren, G., Lord, P., Markhasin, V.S., Matsuoka, S., McCulloch, A.D., Mirams, G.R., Morley, G.E., Nattel, S., Noble, D., Olesen, S.P., Panfilov, A.V., Trayanova, N.A., Ravens, U., Richard, S., Rosenbaum, D.S., Rudy, Y., Sachs, F., Sachse, F.B., Saint, D.A., Schotten, U., Solovyova, O., Taggart, P., Tung, L., Varró, A., Volders, P.G., Wang, K., Weiss, J.N., Wettwer, E., White, E., Wilders, R., Winslow, R.L., Kohl, P., 2011. Minimum Information about a Cardiac Electrophysiology Experiment (MICEE): Standardised reporting for model reproducibility, interoperability, and data sharing. Prog Biophys Mol Biol. 107, 4–10.
Relan, J., Sermesant, M., Delingette, H., Pop, M., Wright, G.A., Ayache, N., 2009. Quantitative Comparison Of Two Cardiac Electrophysiology Models Using Personalisation To Optical And Mr Data. ISBI. 1027–1030.
Relan, J., Pop, M., Delingette, H., Wright, G., Ayache, N., Sermesant, M., in press. Personalisation of a cardiac electrophysiology model using optical mapping and MRI for prediction of changes with pacing, IEEE Trans Biomed Eng.
Relan, J., Chinchapatnam, P., Sermesant, M., Rhode, K., Delingette, H., Razavi, R., Ayache, N., 2010a. Coupled personalisation of electrophysiology models for simulation of induced ischemic ventricular tachycardia, in: Proc. Medical Image Computing and Computer Assisted Intervention (MICCAI'10), LNCS, Beijing, China.
Relan, J., Pop, M., Delingette, H., Wright, G., Ayache, N., 2010b. Sermesant, M. Estimation of reaction, diffusion and restitution parameters for a 3D myocardial model using optical mapping and MRI, in: International workshop on Statistical Atlases and Computational Models of the Heart and Cardiac Electrophysiological Simulation Challenge (STACOM-CESC'10), LNCS 6364, pp. 270–280.
Rogers, J.M., McCulloch, A.D., 1994. A collocation-galerkin finite element model of cardiac action potential propagation. IEEE Trans. Biomed. Eng. 41, 743–757.
Romero, D., Sebastian, R., Bijnens, B., Zimmerman, V., Boyle, P., Vigmond, E., Frangi, A., 2010. Effects of the Purkinje system and cardiac geometry on biventricular pacing: a model study. Ann. Biomed. Eng. 38, 1388–1398.
Roth, B.J., 1997. Electrical conductivity values used with the bidomain model of cardiac tissue. IEEE Trans. Biomed. Eng. 44, 326–328.
Sermesant, M., Moireau, P., Camara, O., Sainte-Marie, J., Andriantsimiavona, R., Cimrman, R., Hill, D., Chapelle, D., Razavi, R., 2006. Cardiac function estimation from MRI using a heart model and data assimilation: advances and difficulties. Med. Image Anal. 10, 642–656.
Sethian, J.A., 1996. A fast marching level set method for monotonically advancing fronts, volume 93, pp. 1591–1595.
Smith, N., de Vecchi, A., McCormick, M., Nordsletten, D., Camara, O., Frangi, A.F., Delingette, H., Sermesant, M., Relan, J., Ayache, N., Krueger, M.W., Schulze, W., Hose, R., Valverde, I., Beerbaum, P., Staicu, C., Siebes, M., Spaan, J., Hunter, P., Weese, J., Lehmann, H., Chapelle, D., Razavi, R., 2011. euHeart: Personalized and integrated cardiac care using patient-specific cardiovascular modelling. J. Royal Soc. Interface Focus 1, 349–364.
Strickberger, S., Conti, J., Daoud, E., Havranek, E., Mehra, M., Peña, I., Young, J., 2005. Patient selection for cardiac resynchronization therapy. Circulation 111, 2146–2150.
ten Tusscher, K.H., Panfilov, A.V., 2006. Alternans and spiral breakup in a human ventricular tissue model. Am. J. Physiol. Heart Circ. Physiol. 291, H1088–H1100.
Vigmond, E.J., Hughes, M., Plank, G., Leon, L.J., 2003. Computational tools for modeling electrical activity in cardiac tissue. J. Electrocardiol. 36 (Suppl), 69–74.
Wang, V., Lam, H., Ennis, D., Cowan, B., Young, A., Nash, M., 2009. Modelling passive diastolic mechanics with quantitative MRI of cardiac structure and function. Med. Image Anal. 13, 773–784.
Wang, L., Zhang, H., Wong, K., Liu, H., Shi, P., 2010a. Physiological-model-constrained noninvasive reconstruction of volumetric myocardial transmembrane potentials. IEEE Trans. Biomed. Eng. 5, 296–315.
Wang, L., Wong, K., Zhang, H., Liu, H., Shi, P., 2011. Noninvasive computational imaging of cardiac electrophysiology for 3D infarct quantitation. IEEE Trans. Biomed. Eng. 58, 1033–1043.
Wang, L., Wong, K., Zhang, H., Liu, H., Shi, P., 2010b. A statistical physiological-model-constrained framework for computational imaging of subject-specific volumetric cardiac electrophysiology using optical imaging and MRI data, in: International workshop on Statistical Atlases and Computational Models of the Heart and Cardiac Electrophysiological Simulation Challenge (STACOM-CESC'10), LNCS 6364, pp. 261–269.
Wong, C.L., Zhang, H.Y., Liu, H.F., Shi, P.C., 2007. Physiome-model-based state-space framework for cardiac deformation recovery. Acad. Radiol. 14, 1341–1349.
Xi, J., Lamata, P., Shi, W., Niederer, S., Land, S., Rueckert, D., Duckett, S., Shetty, A., Rinaldi, A., Razavi, R., Smith, N., 2011. An automatic data assimilation framework for patient-specific myocardial mechanical parameter estimation, in: International Conference on Functional Imaging and Modeling of the Heart (FIMH'11), LNCS 6666, pp. 392–400.
Zimmerman, V., Sebastian, R., Bijnens, B., Frangi, A., 2009. Modeling the Purkinje conduction system with a non deterministic rule based iterative method, in: Computer in Cardiology, volume 36, pp. 461–464.